Phase Structure and Crystallization Behavior of Polypropylene in-Reactor Alloys: Insights from Both Inter- and Intramolecular Compositional Heterogeneity

Haijin Zhu,[†,‡] Benjamin Monrabal,[§] Charles C. Han,[†] and Dujin Wang*,[†]

Beijing National Laboratory for Molecular Sciences, CAS Key Laboratory of Engineering Plastics, Joint Laboratory of Polymer Science and Materials, Institute of Chemistry, Chinese Academy of Sciences, Beijing 100080, China, Graduate School of Chinese Academy of Sciences, Beijing 100080, China, and Polymer Char, Nicholas Copernico 10, P.O. Box 176, E-46980 Paterna, Spain

Received October 19, 2007; Revised Manuscript Received November 24, 2007

ABSTRACT: Systematic investigation on the compositional heterogeneity, phase structure, the crystallization and subsequent melting behavior of two commercial in-reactor alloys EB−P and EP−P (ethylene-*co*-butylene polypropylene and ethylene-*co*-propylene polypropylene) from Basell were conducted. The composition of the alloys and the chain structure of each component were characterized by combinatorial using of preparative TREF and ^{13}C NMR technique. The compositional heterogeneities of both samples were further studied by SSA technique, and possible thermal fractionation mechanisms were then inferred. Correlations between the mechanical properties and the molecular architectures and phase structures were discussed. The results show that the excellent balance between toughness and rigidity of sample EB−P primarily benefits from the crystalline polyethylene homopolymer (HPE) phase and the amorphous ethylene-α-olefin copolymer (EC) component, which is proved to be enriched at the interface between the dispersed polypropylene homopolymer phase (HPP) and the matrix (HPE). As for EP−P sample, the very high amorphous EC content, and the homogeneous and interpenetrating cocontinuous phase structure in the alloy are considered to be mainly responsible for the outstanding low-temperature impact toughness.

1. Introduction

Polypropylene (PP) in-reactor alloys have been widely used as matrix components in automobile parts, appliances, and other industrial uses in the last 2 decades because of the excellent mechanical properties and relatively low production cost.[1] A typical in situ polypropylene blend is prepared by sequential copolymerization of propylene and ethylene-α-olefin mixture over Ziegler−Natta catalysts.[2,3] This technique has long been recognized as a powerful technique to get in situ multiphase polyolefin systems. Actually, no significant progress had been made in this field until the development of spherical, superactive $TiCl_4/MgCl_2$ based catalysts. This together with the so-called "reactor granule technology" make it possible to exploit a series of widely diversified, previously unavailable multiphase materials, PP in-reactor alloys.[4]

Among the ways of toughening PP, the in-reactor blending of PP with ethylene−propylene rubbers (EPR) has been proved to be efficient in improving the inherently poor impact properties of polypropylene. However, the PP/EPR in-reactor alloys generally show very complicated microstructures and typical heterophasic morphology, which consists of rubbery EPR spherical domains dispersed in the semicrystalline polypropylene matrix.[5,6] Since the composition distribution, macromolecular chain structure, molecular weight, and molecular weight distribution of the diverse components in polymer blends have key influence on the morphology and physical properties of the PP alloys,[7,8] a complete understanding of multiscale structure as well as related thermal and mechanical properties for such PP alloys is necessary. Although the compositional heterogeneity and chain structure of traditional PP/EPR in situ blends have been extensively investigated,[5,9−11] little is known about the conclusive relationship among the molecular structure, phase structure and the ultimate mechanical properties due to its extremely complex compositions in such system. The structure similarities between block copolymer and the PE/PP blends also make it difficult to distinguish them.

With the developments of catalyst technology and polymerization process, ethylene-α-olefin copolymers are gradually taking the place of traditionally used EPR to improve the impact resistance of PP.[12−18] In spite of the large amount of reports on such blends, most of the previous work focused on the polymerization and physical property characterization of PP in-reactor alloys with 1-butane, 1-hexene and/or 1-octane based ethylene-α-olefin copolymers.[19−21] There are few systematic comparison investigations on the structure−property relationship of PP/EPR in-reactor alloy and PP/ethylene-α-olefin copolymers. Furthermore, the detailed analysis on the thermal behavior of each component is also very informative in elucidating the correlation between inter- and/or intrachain structure and the multiphase morphology.

Therefore, in the present work we report a critical comparison of the compositional heterogeneity, phase structure and crystallization behavior of two spherical $TiCl_4/MgCl_2$ catalysts based PP in-reactor alloys, PP/EPR and PP/ethylene-α-butylene. The thermal behaviors of each component in both samples will be studied and correlated to the multiscale structure of the in-reactor alloy systems, and possible thermal fractionation mechanism will be inferred. The compatibility between dispersed phase and matrix and the contributions of different components to the

* Corresponding author. Telephone: 86-10-82518533. Fax: 86-10-82612857. E-mail: djwang@iccas.ac.cn.

† Beijing National Laboratory for Molecular Sciences, CAS Key Laboratory of Engineering Plastics, Joint Laboratory of Polymer Science and Materials, Institute of Chemistry, Chinese Academy of Sciences.

‡ Graduate School of Chinese Academy of Sciences.

§ Polymer Char.

10.1021/ma702324h CCC: $40.75
Published on Web 12/29/2007

Table 1. Properties of PP in-Reactor Alloys

sample ID	comonomer type	MFI g/10 min (230 °C/2.16 kg)	density (kg/m^3)	notched Izod impact strength (kJ/m^2) (ISO 180)		flexural modulus (MPa) (ISO 178)	tensile strain (%) at break (ISO 527−1, −2)
				20 °C	−40 °C		
EP−P	propylene	2.5	880	NB[a]	NB	200	570
EB−P	butylene	7.5	890	NB	10	470	>500

[a] The sample was not broken in the test.

overall mechanical properties of the PP-based alloys will be discussed. The possible toughening mechanism is also deduced based on the research results of crystallization and phase separation behaviors in the two PP based alloys.

2. Experimental Section

2.1. Materials. The two PP in-reactor alloys (EP−P, EB−P) used in the present work are commercial products produced by Basell Company using a spherical superactive $TiCl_4/MgCl_2$-based catalyst. The two products can be used as engineering plastics, and show very high efficiency as impact modifiers. The basic parameters and mechanical properties reported by the supplier are summarized in Table 1.

2.2. Crystallization Analysis Fractionation (CRYSTAF) and Temperature Rising Elution Fractionation (TREF). The analytical CRYSTAF and TREF experiments were carried out on a commercial CRYSTAF-TREF instrument (model 200) at Polymer Char Company (Spain). The peculiarity of this equipment is that the TREF apparatus can be easily converted into a fully automated CRYSTAF system and vice versa. A highly sensitive and reliable IR detector that can work at two simultaneous wavelengths was used to measure the concentration and composition of the separated components. In TREF analysis, about 100 mg of polymer was dissolved in 20 mL of *o*-dichlorobenzene (*o*-DCB) at 160 °C for 90 min and stabilized with 300 ppm of butylated hydroxytoluene (BHT) at 130 °C for 45 min. The solution was deposited on a steel column packed with an inert support, and the column was cooled down to room temperature at a rate of 0.5 °C/min. The polymer crystallized during the cooling process was then eluted with *o*-DCB at a heating rate of 1 °C/min, and the concentration of the eluted solution at a 0.5 mL/min flow rate was monitored on-line at the exit by an IR detector. In CRYSTAF process, the solvent used was trichlorobenzene (TCB) and stabilized with 300 ppm of BHT. About 30 mg of polymer was first dissolved in 30 mL of TCB, and then crystallized from 95 to 35 °C at a rate of 0.2 °C/min. The solution concentration was monitored as temperature went down, to obtain the cumulative composition distribution.

The preparative TREF was performed only on EB−P with a Polymer Char PREP mc2 instrument. Xylene stabilized with 600 ppm of Irganox was used as solvent. The temperature segment selected for the fractionation was based on analytical TREF curve, and the effect of solvent on the dissolution temperature was calibrated by standard materials before. Four fractions were collected by fractionating 2 g of EB−P at 30, 87, 96, and >96 °C, respectively. Purified fractions were obtained by concentrating the extracted solutions, precipitating the polymer, and washing and drying the fractions in a vacuum.

2.3. Thermal Analysis and Thermal Fractionation. A Mettler 822e DSC apparatus was used for determining the thermal properties of PP in-reactor alloys. About 2.5 mg of the sample was cut from the pellets and sealed in an aluminum pan. The calibration of the temperature scale and the heat flow was achieved from the melting scans of high-purity indium and zinc samples at the same heating rate. The heat history of the samples was eliminated by holding at 230 °C for 5 min. Subsequently, the samples were cooled to 0 °C at a rate of 10 °C/min, and the thermograms were recorded during the first cooling scan. The melting temperature and fusion enthalpy of the samples were determined during the second heating scan at a rate of 20 °C/min.

Successive self-nucleation and annealing (SSA) was performed according to the following procedure:[22] Samples were first held at 230 °C for 5 min under nitrogen atmosphere and then decreased to 0 °C at a rate of 20 °C/min to create a standard thermal history. Because of the large difference of the melting points between PP component and EP or EB component, SSA procedures were performed separately for the two kinds of components. The self-seeding temperature (T_s), which is thought to be one of the most important parameters in SSA study, was suggested by Mueller to be the minimum temperature of melting domains, in which the temperature is high enough to melt almost all of the polymer crystals but low enough to leave "small" crystal fragments that can act as self-nuclei.[23] Therefore, single-step self-nucleation experiments have been done to determine the melting domains of PP components in both samples.[24] The first T_s for PP components was determined to be 171 °C for EP−P and 169 °C for EB−P samples, respectively. A constant initial T_s of 127 °C was employed for the PE components in the both samples. The fraction window adopted here was 5 °C, and the annealing time was 30 min. The scanning rate used during the thermal conditioning steps was 20 °C/min. Pijpers recently introduced the high-speed calorimetry concept that the increment in heating rate can be compensated by reducing the sample mass.[25] So a higher scanning rate of 20 °C/min was employed to reduce the fractionation time, and a small sample mass of 2.4 mg was used as compensation. The temperature range for thermal fractionation was 151−171 and 149−169 °C for PP components in EP−P and EB−P, respectively, and 87−127 °C for the ethylene-α-olefin copolymer (EC) component in both samples. After completion of the fractionation process, the melting endotherms were recorded at a heating rate of 10 °C/min.

2.4. Nuclear Magnetic Resonance (NMR). ^{13}C NMR spectra were measured on a Bruker dmx300 NMR spectrometer at a resonance frequency of 75.5 MHz. Then, 20 wt % polymer/*o*-dichlorobenzene solutions were prepared with 1 wt % TMS (tetramethylsilane) as internal chemical shift reference. The spectra were recorded at 120 °C and typically 3000 transients were collected. The peak assignments of different carbon atoms along the molecular chain in NMR spectra were according to Zhu.[26]

2.5. Scanning Electron Microscopy (SEM). The sample pellets were hot-pressed into bars and then cryofactured under liquid nitrogen. The fracture surface was etched in xylene for 6 h at different temperatures, and then coated with platinum, and finally submitted to SEM observations on a JEOL JSM-6700F field emission scanning electron microscope. An operating voltage of 10 kV and magnification of 5000 were used for observation.

3. Results and Discussion

3.1. Composition and Chain Structure Characterization. Characterization of the chain structure and composition of multicomponent polyolefin in-reactor alloys is critical to the fundamental understanding of the interactions among the components and the toughening mechanisms. Therefore, ^{13}C NMR spectroscopy measurement of EP−P and EB−P were first performed in order to clarify their composition and chain structure, and the results are summarized in Table 2. In sample EP−P, the content of triad EEE (29.2 mol %) is considerably smaller than that of triad PPP (37.6 mol %), though the monomer contents of P and E are basically the same (ca. 50 mol %). Such results indicate that there is more propylene

Table 2. Sequence Distribution and Monomer Content (mol %) in EP−P and EB−P Obtained by ^{13}C NMR

EP−P	P	E	PP	PE	EE	PPP	PPE	PEP + EPE	EEP	EEE
	50.3	49.7	41.6	22.2	36.2	37.6	7.9	11.6	13.8	29.2

EB−P	P	E	B	EE	EB	BB
	28.8	67.4	3.8	94.7	5.3	0

homopolymer (HPP) and long sequence segmented PP than its PE counterpart, but less the short segmented PP than the short segmented PE. It is also interesting to notice that the content of triad EEP, however, is higher than that of PPE. The above result is understandable as the polymerization process of the alloys is considered. The in-reactor alloy is synthesized by first polymerizing propylene to form spherical HPP granules in the first stage, and then polymerizing ethylene in the second stage, during which copolymerization between ethylene and propylene occurs simultaneously. As the catalyst system is fixed, by controlling the kinetics of homopolymerization and copolymerization in the preparation process of PP in-reactor alloys, the composition and chain sequence are tunable. In the case of EB−P, no EP or BP sequences were detected, meaning that the PP component only exists as homopolymer in the complex system. So, it can be inferred from the NMR results that the EB−P sample is composed of HPP, linear low-density polyethylene (LLDPE) with broad distribution of butylene comonomer in the polymer chain, and probably some polyethylene homopolymer (HPE).

In order to further illustrate the compositions of the two in-reactor alloys, analytical TREF and CRYSTAF were performed. The CRYSTAF method was proved to be insensitive in these analyses because the larger undercooling of PP over PE results in solution crystallization under very close temperatures and only one broad peak can be found in the CRYSTAF curves. TREF, however, turned out to be efficient in fractionating the PP in-reactor alloys. The TREF curves of sample EP−P and EB−P are shown in Figure 1. It can be seen that there are several well resolved peaks in the curves of both samples, indicating that the in-reactor alloys are composed of several components. A large number of investigations have been published on the macromolecular structure of PP/PE in-reactor alloys.[5,27−33] According to the previous research, the peaks in TREF curve of EP−P are assigned as follows: F1, ethylene−propylene random copolymer; F2, ethylene homopolymer and ethylene−propylene segmented copolymer with long ethylene sequence; and F3, propylene homopolymer and small amount of ethylene−propylene-segmented copolymer with a long propylene sequence. However, up to date there are very few reports on the microstructure, structure distribution and structure-properties relationship of iPP/ethylene−butylene copolymer alloys, which are prepared based on spherical catalysts.

Generally, it is difficult to confirm whether HPE component exists in the EB copolymer or not because of the similarity of both structure and property between HPE and PE segment in copolymer as the content of comonomer unit (butylene) is relatively low in the polymer chain. However, the simultaneous use of preparative TREF and ^{13}C NMR spectroscopy can be very informative in elucidating the compositional heterogeneity of polyolefins and the chain structure of each component. The 13C−NMR spectra of sample EB−P fractions are presented in Figure 2, and the related data are summarized in Table 3. It can be seen that F1 is a LLDPE fraction with relatively short ethylene sequence length, F2 mainly composed of the LLDPE with longer ethylene sequence length and maybe also some HPE, F3 mainly corresponding to HPE, and F4 HPP. The very small amount of HPE in F4 and F2, and HPP in F3 and F2 are contaminations from the fraction procedure. The above speculation can be testified by the analytical TREF experiments on each fraction obtained by preparative TREF. As shown in Figure 3, the TREF curve of each fraction shows more than one peak, indicating that besides the main component, small contaminations were also present. From this analysis, it can be confidently concluded that sample EB−P is composed of HPP, HPE and ethylene−butylene copolymer with various ethylene sequence lengths. No ethylene−propylene copolymer or butylene-propylene copolymer exists in this complex in-reactor alloy system.

3.2. Thermal Properties. Figure 4 shows the typical DSC curves for the two PP in-reactor alloys EB−P and EP−P. It is noticed that, for sample EB−P, the two lower temperature peaks corresponding to the crystallization and melting all split into two peaks, which might be assigned to the two components, HPE (F3) and LLDPE (F2), respectively. The previous analytical results from preparative TREF and NMR spectroscopy have also proved the existence of both HPE and LLDPE with long ethylene sequence length. As the area of DSC curves is normalized by the total sample weight, the content of crystalline components in polymers can be represented by the area of melting peaks. As can be seen from Figure 4b, the area under the melting curves of PP components is almost equivalent for the two samples, indicating that EP−P and EB−P contain

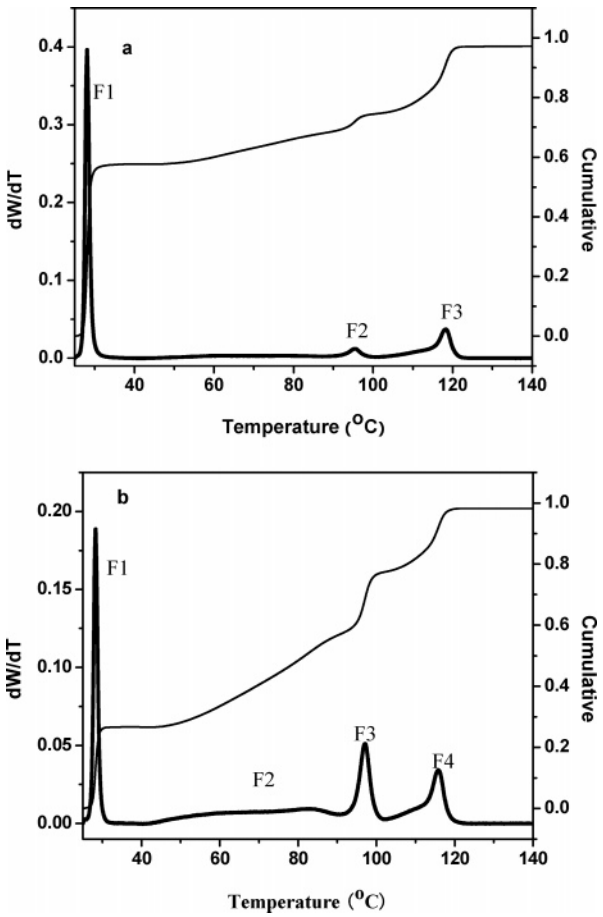

Figure 1. Analytical TREF curves of the PP in-reactor alloys: (a) EP−P; (b) EB−P.

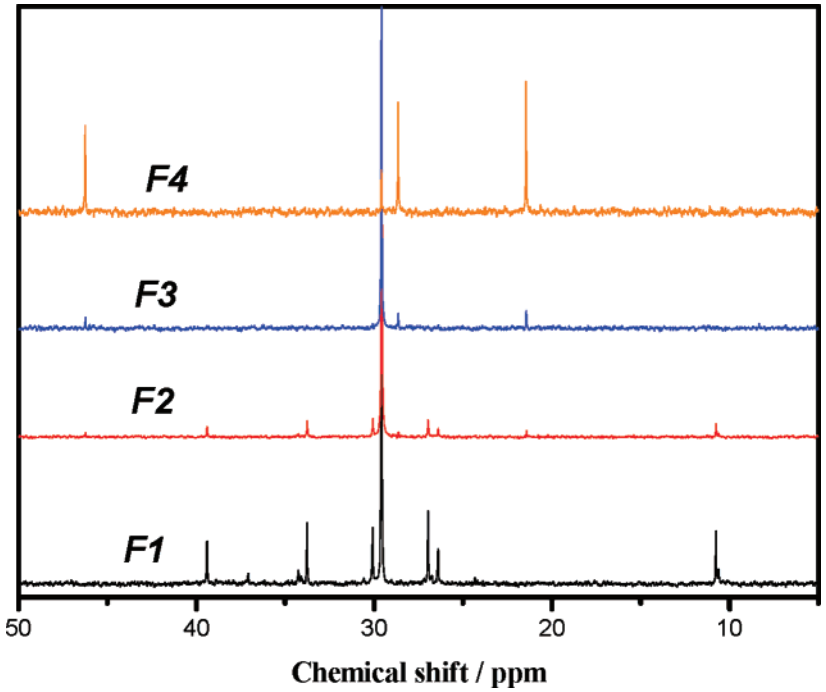

Figure 2. ^{13}C NMR spectra of EB−P fractions obtained by preparative TREF. Extraction temperatures for F1, F2, F3, and F4 were 30, 87, 96, and >96 °C, respectively.

Table 3. Composition and Microstructure of Sample EB−P Obtained by Preparative TREF and ^{13}C NMR

Fractions	F1		F2			F3		F4	
Temperature range	T<30°C		30 °C<T<87 °C			87 °C <T<96 °C		T>96 °C	
Peak temperature in analytical TREF	28 °C		97°C, 89.9 °C, 28°C			97 °C		116 °C, 97 °C	
Content of fractions from TREF (wt.%)	27.2		30.8			21.0		21.1	
Composition	LLDPE with short ethylene sequence		LLDPE with long ethylene sequence (few HPP and HPE)			HPE (few HPP)		HPP (few HPE)	
Comonomer	B	E	P	B	E	P	E	P	E
Monomer content (mol %)	16.1	83.9	3.0	5.3	91.7	7.6	92.4	86.2	13.8

comparable crystalline PP component. Nevertheless, the content of crystalline EP copolymer in EP−P is much less than that of the crystalline EB copolymer in EB−P. It is also noted that although the melting temperature of the EC components are identical, their crystallization temperature and crystallization rate are remarkably different. The EC component in sample EB−P crystallizes at much lower temperature, and its crystallization rate is also obviously slower than that of EP−P. This result together with the previously observed overlapped peaks in endotherms and exotherms of EC component in EB−P, could probably lead to interpretation of partial miscibility between the HPE and ethylene−butylene copolymer. This effect could be interpreted as the nucleation effect of HPE crystals on the crystals of branched PE, the dilution effect of the molten branched EC chains on the crystals formed by the more linear PE, and finally possible partial miscibility.

SSA is essentially a thermal fractionation method, which is based on the sequential application of self-nucleation and annealing steps on polymer samples. It can give information on the distribution of short chain branching and lamellar thickness. To further investigate the composition distribution, including molecular chain branching distribution of EC component and the stereodefects of PP component, SSA technique was used. Figure 5 shows the DSC endotherms of the PP component of EP−P and EB−P samples after having been subjected to a five-step SSA treatment, with the following

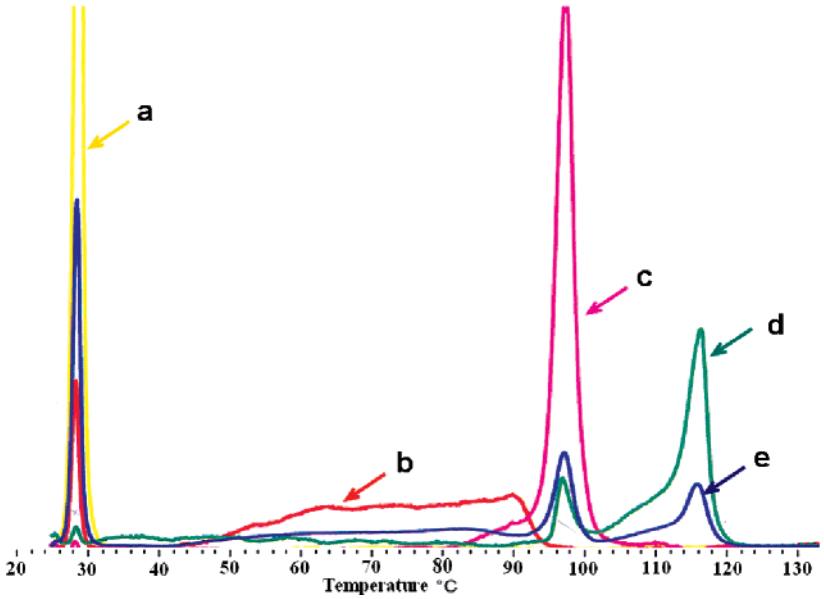

Figure 3. Analytical TREF curves of sample EB−P and the four fractions: (a) F1; (b) F2; (c) F3; (d) F4; (e) EB−P.

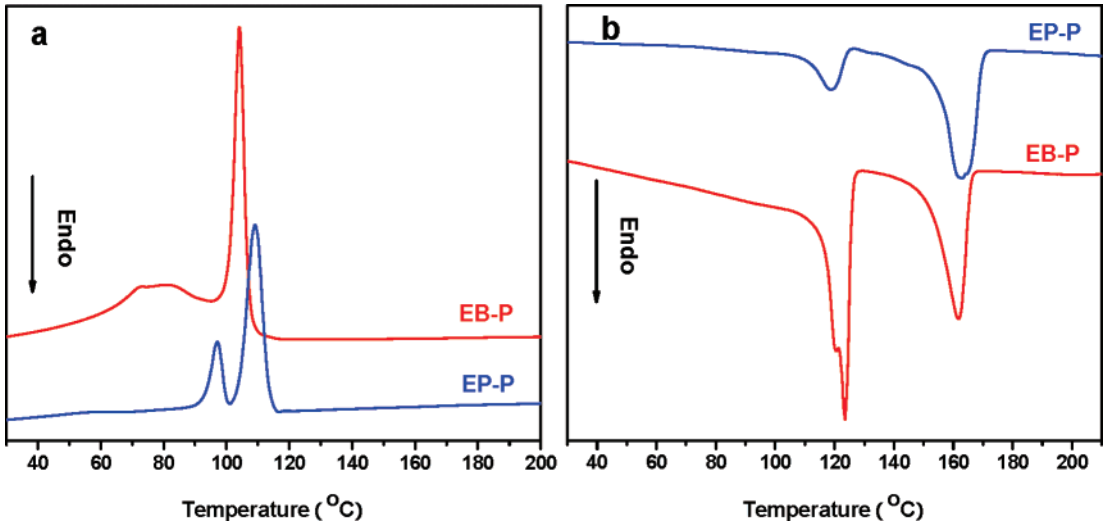

Figure 4. DSC crystallization (a) and melting (b) curves of the two PP in-reactor alloys.

processing temperatures for self-nucleation and annealing: 171, 166, 161, 156, and 151 °C for EP−P and 169, 164, 159, 154, and 149 °C for EB−P, respectively. The lower self-seeding temperature of sample EB−P can be probably ascribed to its lower molecular weight. This speculation can be further supported by the higher MFI value in Table 1, though it cannot be taken as sufficient evidence.

The series of melting endotherms observed in the DSC heating scans indicate that thermal fractionation has occurred during the SSA treatment (Figure 5). The fractions that exhibit the highest melting points are those with the longest linear or isotactic segments incorporated within the specific lamellar population and therefore they would be the ones with the lowest defects concentration. Since the first self-seeding temperature does not cause any annealing or lamellae thickening because it is a T_s temperature within HPP domains, only four steps were able to produce annealing. Detailed examination reveals that the melting trace of EP−P shows the melting of four fractions corresponding to the four annealing steps; the melting trace of EB−P, nevertheless, shows only three melting peaks. It is also very interesting to notice that the first two melting peaks (labeled as 1 and 2 in Figure 5) of both the samples are separated very well with each other. The other peaks, however, are less

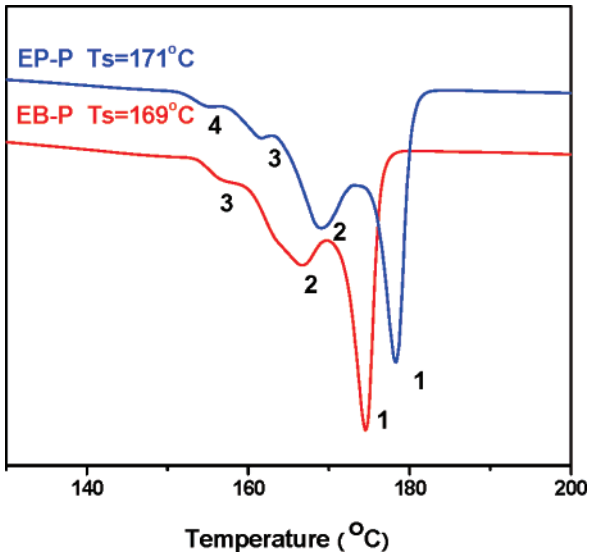

Figure 5. DSC endotherms of PP component after SSA treatment.

resolved. We believe that the first two peaks were not segregated just by the molecular chain defects but also by some contribution

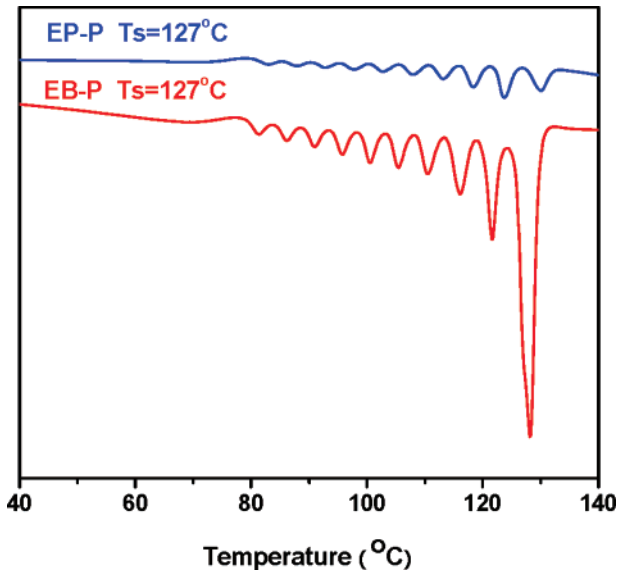

Figure 6. DSC endotherms of EC component after SSA treatment.

from the melting−recrystallization-remelting process during heating, as will be discussed later. So, it may not provide much information about crystalline sequence length distribution. As has been demonstrated previously, the SSA procedure fractionates the polymer mainly by the defects on the polymer chain with a minor influence of the molecular weight distribution.[34,35] The nature of the polymer chain must be heterogeneous in order to have a wide distribution of crystallizable chain segments. If SSA is performed on a perfectly linear HDPE with wide polydispersity, almost no fractionation is obtained. The effect of molecular mass distribution on the fractionation is therefore limited.

The results of Figure 5 indicate that the neat HPP component in sample EB−P is very difficult to fractionate in view of its negligible branching content or steric defects as indicated by NMR data. The profile of the two melting endotherms for the two samples looks very similar at the first sight, however, the intrinsic fractionation mechanisms for the PP components in the two samples should be very different. Considering the negligible steric defects for both samples as suggested by NMR data, the SSA procedure fractionates the sample EP−P mainly by its compositional heterogeneity. In the case of sample EB−P, however, it is likely to be fractionated by molecular weight because there are neither compositional defects nor steric defects presented in the polymer chains. It is well-known that the crystallization and melting temperatures depend strongly on molar mass with samples having molar mass below 10000, though the presence of weakly resolved peaks in the DSC endotherm helps to indicate that the process of segregation by SSA is insensitive to the differences in molecular weight. The weight-average molar mass is higher than 10000, but the lower molar mass part is in the range that should show a molar mass dependent signal in SSA.

The results from the SSA measurements of the EC component of sample EP−P and EB−P are presented in Figure 6. Multiple melting peaks can be seen which are formed during each step of annealing. Each endotherm represents a population of crystals with almost the same thermodynamic stability. As the normalized differential area under each endothermic peak is proportional to the number of lamellae that melt with the temperature interval considered, the lamellae thickness and crystalline methylene sequence length (CMSL) and their distributions can thus be calculated. According to Sanchez and Eby,[36] the relationship between the melting temperature T and lamellae thickness l of random copolymer with composition X (molar fraction of ethylene monomer) can be expressed as follows:

$$T = T_m^c\left(1 - \frac{2\gamma\sigma_e}{\Delta H_u l}\right) \tag{1}$$

Here

$$\frac{1}{T_m^c} = \frac{1}{T_m^0} - \frac{R}{\Delta H_u}\ln X \tag{2}$$

where T_m^0 is the melting point for the perfect crystal (418.7 K for polyethylene),[37] and ΔH_u is the heat of fusion for a repeat unit (8.28 kJ/mol for C_2H_4 units in polyethylene),[38] σ_e the basal surface energy (90 mJ/m^2 for polyethylene),[38] γ the molar volume of a repeat unit in the perfect polyethylene crystal (2.79×10^{-5} m^3/mol).[39]

In this method, the melting temperatures are used to calculate the lamellae thickness. For low-temperature fractions formed by short methylene sequences, the lamellae thickness is equal to CMSL; however, where high-temperature fractions are concerned, the lamellae thickening occurs and the methylene sequence is long enough to fold in the same crystal; thus, the lamellae thickness is smaller than its corresponding CMSL. In other words, one of the limitations of this method is that it cannot calculate the CMSL for high-temperature fractions.

The CMSL for each fraction can be easily calculated by Keating's method:[40]

$$-\ln(X) = -0.331 + 135.5/T_m \tag{3}$$

$$\mathrm{CMSL} = 0.2534X/(1 - X) \tag{4}$$

It should be pointed out that the crystallization of a short chain branched polyethylene may differ from that of linear paraffin used as a model in the Keating method. However, the use of linear paraffin as a reference appears to provide useful information in some cases,[41,42] in the absence of better standard references.

The statistical terms arithmetic mean $\bar{L}_n$, weighted mean $\bar{L}_w$, and the broadness index were first introduced by Keating to describe the polydispersity index I of CMSL of ethyl-based copolymers:[40]

$$\bar{L}_n = \frac{n_1L_1 + n_2L_2 + \ldots + n_iL_i}{n_1 + n_2 + \ldots + n_i} = \sum f_iL_i \tag{5}$$

$$\bar{L}_w = \frac{n_1L_1^2 + n_2L_2^2 + \ldots + n_iL_i^2}{n_1L_1 + n_2L_2 + \ldots + n_iL_i} = \frac{\sum f_iL_i^2}{\sum f_iL_i} \tag{6}$$

$$I = \bar{L}_w/\bar{L}_n \tag{7}$$

where n_i is the normalized peak area, and L_i is the CMSL or lamellae thickness for each fraction. The three terms of ethylene sequence length and lamellae thickness for the EC components are given in Table 4. The broadness indexes of EP−P are larger than those of EB−P sample, and the broader distribution of CMSL in EP−P directly leads to the wider melting temperature regime (see Figure 4b). For both samples, the broadness indexes of CMSL are larger than those of the lamellae thickness. This is understandable when considering two factors: first, some of the chain defects were excluded from the crystals in the process of crystallization fractionation; second, some of the longer

Table 4. Parameters of Polydispersity of EC Components for Both EP−P and EB−P Samples

		methylene sequence length			lamellae thickness		
sample	comonomer type	$\bar{L}_n$ (nm)	$\bar{L}_w$ (nm)	I	$\bar{L}_n$ (nm)	$\bar{L}_w$ (nm)	I
EP−P	propylene	18.4	32.0	1.74	9.5	11.7	1.23
EB−P	butylene	19.8	29.7	1.50	10.1	12.2	1.21

methylene sequences are long enough to fold in the same crystal. It is also noted that although the melting temperature of the fractions of sample EP−P is systematically higher than that of the sample EB−P (Figure 6), its arithmetic mean CMSL and lamellae thickness are smaller. This is probably caused by two factors. One is that the HPE component existing in EB−P contributes to the area of higher melting peaks, thus the population of relatively thicker lamellae with higher melting temperature in sample EB−P is significantly larger than that of sample EP−P. The other factor that may affect the CMSL value is molecular weight. When molecular weight is high enough, the effect of chain entanglement is so important that it cannot be ignored; therefore, this tendency should be also partially due to the chain entanglement with increasing molecular weight. It should also be noted that the SSA technique only detects the defects distribution of ethylene sequences long enough to crystallize, and the sequences too short to crystallize cannot be detected. This result indicates that the polydispersity of CMSL in the real system is quite complicated, and there is still a lot of work to do to understand the real complex systems.

3.3. Phase Morphology. Figure 7 shows the SEM micrographs of cryofractured surface of both molded samples. The phase morphology of unetched samples (Figure 7a) show that obvious phase separation can be observed for sample EB−P, and the dimension of the dispersed phase is about 1−4 μm; the phase morphology of EP−P, however, is much flatter and much more homogeneous. As can be seen from the morphology of etched samples, EP−P exhibits characteristic cocontinuous phase at the scale of several microns. The excellent percentage elongation at break and impact strength properties may arise as a consequence of this interpenetrating network structure. For sample EB−P, it can be judged from combination of the analytical TREF and the morphology of the samples etched at different temperatures that the spherical dispersed phase is HPP, and the prominent globular granules are dispersed in an HPE matrix. It is also noted that in the micrograph of the unetched sample, the dispersed phase is wrapped tightly by the matrix. After the samples were etched at room temperature, however, obvious gap can be observed between the globular granules and the matrix. It may suggest that the gaps between the dispersed phase and the matrix are formed by dissolution of the amorphous EC component, which is expected to be dissolved in xylene at room temperature. In other words, the amorphous EC component exists as an interphase between the crystalline HPP domains and the crystalline HPE matrix. Detailed examination of the micrograph of sample EB−P in Figure 7b can also reveal that there are something like thin threads with diameters of several nanometers between the granules and the matrix, indicating interfacial adhesion between the dispersed phases and the matrix. Such morphology is exclusive for the in-reactor alloys,[43,44] which may at least partially account for its excellent impact toughness.

3.4. Mechanical Properties. It is well-known that, for multiphase polymer systems, the toughening effect is mainly determined by two factors. The first one is the size of the dispersed phase and its distribution. It is generally accepted that

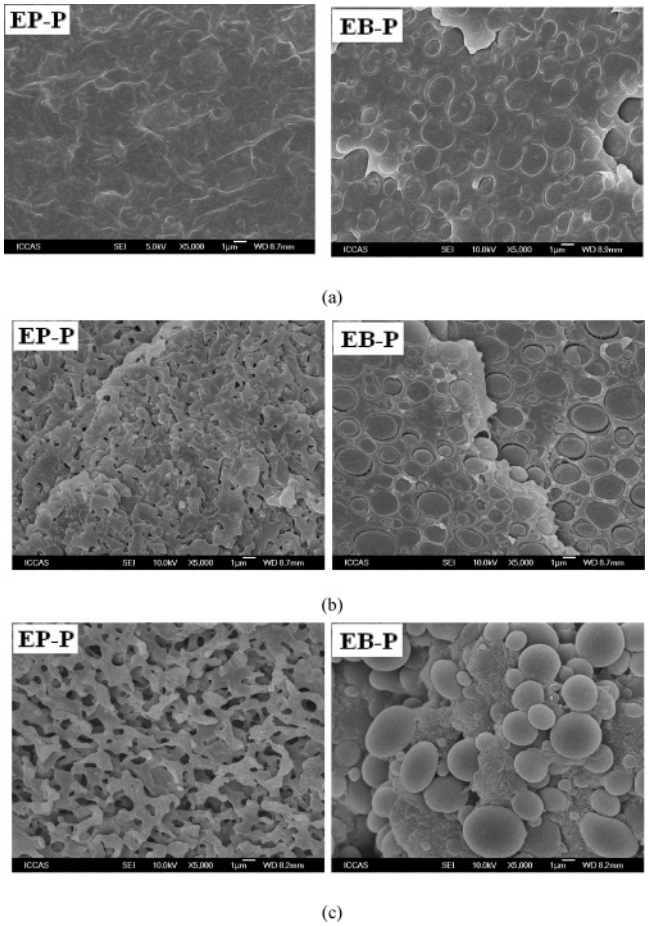

Figure 7. SEM micrographs of fracture surface of samples EP−P and EB−P at magnification of 5000: (a) unetched; (b) etched at room temperature; (c) etched at 85 °C.

the impact toughness will increase as the size of the dispersed phase (particle) and its distribution broadness index getting smaller. The small and narrow distributed particles usually come from small surface tension between the matrix and the particles, which mean good compatibility between different phases in the multiphase system. The second factor is the interfacial adhesion between the particles and the matrix. The SEM results of sample EB−P prove that although the HPP phase is completely separated with the HPE phase, the amorphous EC component existing between the dispersed phase and matrix can act as a compatilizer. Thus, the coexistence of crystalline HPE phase and amorphous EC phase in the PP in-reactor alloy leads to the macroscopically homogeneous but microscopically separated phase structure, which ultimately improve the impact toughness significantly without sacrificing the flexural modulus very much (see Table 1). Such good balance between toughness and rigidity is very important for the applications of PP in-reactor alloys as high-performance structural materials. Moreover, the sample EP−P, as shown in Table 1, shows superior low-temperature impact strength. This could be explained from two aspects: First, from the phase structure point of view, the advanced low-temperature impact strength of sample EP−P could be ascribed to the interpenetrate network microstructure; second, from the molecular composition point of view, its excellent low-temperature impact toughness could be attributed to the large content of ethylene−propylene copolymer (including the random and segmented copolymer), as well as the good compatibility between different components in the complex in-reactor alloy system.

4. Conclusions

The compositional heterogeneity, phase structure and melting behavior of two spherical $TiCl_4/MgCl_2$ catalysts based PP in-reactor alloys were studied by a combinatory investigation of NMR, TREF, DSC, and SEM techniques. It has been found that the sample EB−P is composed of HPP, HPE, and ethylene−butylene copolymer with different ethylene segment lengths, while sample EP−P is mainly composed of HPP, E−P segmented copolymer, and E−P random copolymer.

The possible thermal fractionation mechanism of the PP and EC components of the samples were inferred. SSA procedure fractionates PP component of the sample EP−P mainly by its compositional heterogeneity. In the case of sample EB−P, however, it is likely to be fractionated by molecular weight. The CMSL and lamellae thickness and their distribution broadness index of the EC components in both samples are also studied by SSA technique. The higher HPE content and lower molecular weight of sample EB−P are mainly responsible for the larger arithmetic mean CMSL and lamellae thickness.

Correlations between the molecular architectures, phase structures and the ultimate mechanical properties were constructed. The excellent balance between toughness and rigidity of sample EB−P is primarily achieved by the macroscopically homogeneous but microscopically phase-separated structure. The amorphous EC component was proved to be enriched at the interface between the dispersed phase and the matrix and act as a compatilizer. The advanced low-temperature impact toughness of sample EP−P could be interpreted as a consequence of the high ethylene−propylene copolymer content and the good compatibility between the components in the cocontinuous phase system.

References and Notes

(1) Nomura, T.; Nishio, T.; Iwanami, K.; Yokomizo, K.; Kitano, K.; Toki, S. *J. Appl. Polym. Sci.* **1995**, *55*, 1307−1315.
(2) Galli, P.; Vecellio, G. *Prog. Polym. Sci.* **2001**, *26*, 1287−1336.
(3) Heggs, T. G. *Block Copolymers*; APPl. Sci. Publ. Ltd: London, 1973; pp 493−531.
(4) Galli, P.; Haylock, J. C. *Prog. Polym. Sci.* **1991**, *16*, 443−462.
(5) Cai, H. J.; Luo, X. L.; Ma, D. Z.; Wang, J. M.; Tan, H. S. *J. Appl. Polym. Sci.* **1999**, *71*, 93−101.
(6) Mirabella, F. M. *Polymer* **1993**, *34*, 1729−1735.
(7) Cai, H. J.; Luo, X. L.; Chen, X. X.; Ma, D. Z.; Wang, J. M.; Tan, H. S. *J. Appl. Polym. Sci.* **1999**, *71*, 103−113.
(8) Feng, Y.; Hay, J. N. *Polymer* **1998**, *39*, 6589−6596.
(9) Maruscelli, E. *Thermoplastic Elastomers from Rubber-Plastic Blends*; Ellis Horwood: New York, 1990; pp 28−70.
(10) Feng, Y.; Hay, J. N. *Polymer* **1998**, *39*, 6723−6731.
(11) Randall, J. C. *J. Polym. Sci., Part A: Polym. Chem.* **1998**, *36*, 1527−1542.
(12) Da Silva, A. L. N.; Rocha, M. C. G.; Coutinho, F. M. B.; Bretas, R.; Scuracchio, C. *J. Appl. Polym. Sci.* **2000**, *75*, 692−704.
(13) DaSilva, A. L. N.; Tavares, M. I. B.; Politano, D. P.; Coutinho, F. M. B.; Rocha, M. C. G. *J. Appl. Polym. Sci.* **1997**, *66*, 2005−2014.
(14) Dharmarajan, N. R.; Yu, T. C. *Plastics Eng.* **1996**, *52*, 33−35.
(15) Kukaleva, N.; Cser, F.; Jollands, M.; Kosior, E. *J. Appl. Polym. Sci.* **2000**, *77*, 1591−1599.
(16) Kukaleva, N.; Jollands, M.; Cser, F.; Kosior, E. *J. Appl. Polym. Sci.* **2000**, *76*, 1011−1018.
(17) McNally, T.; McShane, P.; Nally, G. M.; Murphy, W. R.; Cook, M.; Miller, A. *Polymer* **2002**, *43*, 3785−3793.
(18) Yu, T. C. *Polym. Eng. Sci.* **2001**, *41*, 656−671.
(19) Yamaguchi, M.; Miyata, H. *Macromolecules* **1999**, *32*, 5911−5916.
(20) Yamaguchi, M.; Miyata, H.; Nitta, K. H. *J. Appl. Polym. Sci.* **1996**, *62*, 87−97.
(21) Yamaguchi, M.; Miyata, H.; Nitta, K. H. *J. Polym. Sci., Part B: Polym. Phys.* **1997**, *35*, 953−961.
(22) Arnal, M. L.; Sanchez, J. J.; Muller, A. J. *Polymer* **2001**, *42*, 6877−6890.
(23) Arnal, M. L.; Balsamo, V.; Ronca, G.; Sánchez, A.; Müller, A. J.; Cañizales, E.; Navarro, C. U. d. *J. Therm. Anal. Calorim.* **2000**, *59*, 451−470.
(24) Müller, A. J.; Arnal, M. L. *Prog. Polym. Sci.* **2005**, *30*, 559−603.
(25) Pijpers, M. F. J.; Mathot, V. B. F.; Goderis, B.; Scherrenberg, R. L.; van der Vegte, E. W. *Macromolecules* **2002**, *35*, 3601−3613.
(26) Zhu, S. N. *Macromolecular Chain Structure.* Science Press: Beijing, 1996; p 289.
(27) D'Orazio, L.; Cecchin, G. *Polymer* **2001**, *42*, 2675−2684.
(28) Jang, G. S.; Cho, W. J.; Ha, C. S.; Kim, W.; Kim, H. K. *Colloid Polym. Sci.* **2002**, *280*, 424−431.
(29) Xu, J.; Feng, L. *Polym. Int.* **1998**, *47*, 433−438.
(30) Xu, J.; Fu, Z.; Fan, Z.; Feng, L. *Eur. Polym. J.* **2002**, *38*, 1739−1743.
(31) Zacur, R.; Goizueta, G.; Capiati, N. *Polym. Eng. Sci.* **1999**, *39*, 921−929.
(32) Zheng, Q.; Shangguan, Y.; Yan, S.; Song, Y.; Peng, M.; Zhang, Q. *Polymer* **2005**, *46*, 3163−3174.
(33) Fu, Z.; Fan, Z.; Zhang, Y.; Xu, J. *Polym. Int.* **2004**, *53*, 1169−1175.
(34) Müller, A. J.; Hernandez, Z. H.; Arnal, M. L.; Sánchez, A. *J. Polym. Bull. (Berlin)* **1997**, *39*, 465−472.
(35) Arnal, M. L.; Sánchez, J. J.; Muller, A. J. *SPE-ANTEC, NY*; 1999; SPE: New York, 1999; pp 2329−2333.
(36) Sanchez, I. C.; Eby, R. K. *Macromolecules* **1975**, *8*, 638−641.
(37) Flory, P. J.; Vrij, A. *J. Am. Chem. Soc.* **1963**, *85*, 3548−3553.
(38) Hoffman, J. D.; Miller, R. L. *Polymer* **1997**, *38*, 3151−3212.
(39) Howard, P. R.; Crist, B. *J. Polym. Sci., Part B: Polym. Phys.* **1989**, *27*, 2269−2282.
(40) Keating, M.; Lee, I. H.; Wong, C. S. *Thermochim. Acta* **1996**, *284*, 47−56.
(41) Kong, J.; Fan, X.; Xie, Y.; Qiao, W. *J. Appl. Polym. Sci.* **2004**, *94*, 1710−1718.
(42) Zhang, F.; Liu, J.; Fu, Q.; Huang, H.; Hu, Z.; Yao, S.; Cai, X.; He, T. *J. Polym. Sci., Part B: Polym. Phys.* **2002**, *40*, 813−821.
(43) D'Orazio, L.; Mancarella, C.; Martuscelli, E.; Cecchin, G.; Corrieri, R. *Polymer* **1999**, *40*, 2745−2757.
(44) Tan, H. S.; Li, L.; Chen, Z. N.; Song, Y. H.; Zheng, Q. *Polymer* **2005**, *46*, 3522−3527.

MA702324H